A Non-hydrostatic Model for Simulating Dam-Break Flow Through Various Obstacles

Komang Dharmawan[1] **Putu Veri Swastika**[1,✉] **G K Gandhiadi**[1]**, Sri Redjeki Pudjaprasetya**[2]

[1]Department of Mathematics, Faculty of Mathematics and Natural Sciences, Udayana University, Jl. Raya Kampus UNUD, Bukit Jimbaran, Kuta Selatan, Badung 803611, Bali, Indonesia
[2]Industrial and Financial Mathematics Research Group, Faculty of Mathematics and Natural Sciences, Institut Teknologi Bandung, Jalan Ganesha 10, Bandung 40132, Indonesia
veriswastika@unud.ac.id[✉]

Abstract

In this paper, we develop a mathematical model for modelling and simulation of the dam-break flow through various obstacles. The model used here is an extension of one-layer non-hydrostatic (NH-1L) model by considering varying channel width (Saint Venant). The capability of our proposed scheme to simulate free surface wave generated by dam-break flow through various obstacles is demonstrated, by performing two types of simulation with various obstacles, such as; bottom obstacle and channel wall contraction. It is shown that our numerical scheme can produce the correct surface wave profile, comparable with existing experimental data. We found that our scheme demonstrates the evolution of a negative wave displacement followed by an oscillating dispersive wave train. These well-captured dispersive phenomena, indicated both the appropriate numerical treatment of the dispersive term in our model and the performance of our model.

1 Introduction

Dams around the world are plagued by the potential threat of failure which may cause calamities. These calamities are characterized by a sudden, fast, and uncontrolled flow, which is usually caused by structural collapse due to old age or natural disasters. The ensuing floods downstream of a dam can inflict significant damage along their pathways, often resulting in loss of life and destruction of property. Dam failures can pose major issues long after the initial flood has stopped in some circumstances.

On March 27, 2009, the Situ Gintung dam collapsed, which was one of the worst dam collapse occurrences in Indonesia. This 10-meter-high dam is located in Cirendeu, South Tangerang, Banten, and one of the causes that contributed to its collapse was the dam's old age and excessive rainfall outflow. The amount of water that poured downstream at the time of the catastrophe was up to 1 million m^3, inundating areas along the pathways, inflicting damage to public buildings, and killing 100 people. In order to prevent similar incidents in the future, it is necessary to do disaster mitigation in ways such as modelling and simulating dam breaches using mathematical models, which were developed by several authors [4, 19, 13, 30, 8].

The floods due to the dam break exhibit the typical features of open channel flow in that the horizontal length scale is greater than the depth scale, allowing the vertical component of velocity to be ignored. This model is referred to as the hydrostatic model. In our previous work [26, 25], we have successfully studied dam break flow for various obstacles, i.e bottom obstacle [26] and channel wall contraction as an obstacle [25]. Our preceding results using hydrostatic model are quite comparable with other existing results, but the absence of the hydrodynamic pressure term can causes some differences to be found which lead to unrealistic results [9], thus the hydrodynamic pressure term can not be ignored [10]. To address this issue, some researchers propose utilizing different models that can account for dispersive effects, such as the Reynolds-Averaged Navier-Stokes [7, 17, 5] and Boussinesq-type waves model [15, 29, 21, 3]. The acquired findings are quite convincing, but they are difficult, time-consuming, and energy-consuming. Mixed high-order derivative variables in Boussinesq, for example, need specific attention in their discretization [6, 28].

The utilization of neural networks as surrogate models in various real-world engineering scenarios [11], which continues to be developed can be an alternative solution. For example, Kudela and Matousek [12] proposed Surrogate-Assisted Evolutionary Algorithms (SAEAs) based on a Lipschitz underestimation to develop a differential evolution based algorithm. Cai et al. [2] uses the conventional Physic Informed Neural Networks (PINN) to solve various inverse problem in biomedical flow. Tang et al. [27] develops conventional PINN combined with polynomial interpolation

to solve fluid mechanics. Sun et al. [23] modifies conventional PINN into a new Residual Cooperative Neural Network (RCNN) to solve hydrodynamics cases. Al-Ghosun et al. [1] use Proper Orthogonal Decomposition (POD) Polynomial Chaos Expansion (PCE) as a surrogate model to quantify the uncertainty in hydraulic, including the case of dam-break over flat bed. Lund et al. [24] used reservoir-based surrogate forecast model directly constructed from 1D Hydrodynamic model and combined with Ensemble Kalman Filter (EnKF) to forecast flows and overflows in urban area. Further, Nguyen et al. [16] predicted the non-linear hydrodynamic pressure coefficient on submerged bodies near the water surface using surrogate model based on 2D Reynolds-averaged Navier Stokes (RANS) combined with Gaussian process. Both of their results looks promising although the implementation of surrogates model sometimes does not cover the full features of the 1D Hydrodynamic, for example backwater effects, numerical stability issues [24], flow induced instability [16], non-linearity effect [1]. Moreover, the high computational cost of ensemble for hydrodynamic models is also unavoidable [24]. Considering the limitations of the surrogate model for the hydrodynamic case, thus the conventional approach using the Non-Linear Shallow Water (NLSWE) equations with hydrodynamic pressure terms as in [28, 18, 22] still looks promising.

In practice, open channel geometry is quite complicated, necessitating the consideration of varying channel widths, which are not present in the previous study [28, 18]. Thus, in this study, we propose a one-layer non-hydrostatic Saint Venant model. This is an extension of the one-layer non-hydrostatic model (NH-1L) used by Tarwidi et al. [28] to investigate the landslide-generated waves and also considered in [18] to investigate the bottom motion that generates surface waves. The non-hydrostatic model used in the previous research [28, 18] is an improved conservative staggered scheme for NLSWE described previously in [22], to capture the dispersion effects by solving the Euler equations. The MCS scheme used in the implementation of NH-1L is known to be very efficient, easy to implement and robust. In the case hydrostatic variant, without the hydrodynamic pressure term, the MCS scheme is proven to be stable and non-dissipative. Good ability to capture the hydraulic jump, dispersive effects and near steady state condition are a distinct advantage in using this momentum conservation principle in staggered scheme.

Thus, the paper is organized as follows. The governing equations is one-layer non-hydrostatic Saint Venant equations which is discussed in Section 2. In Section 3, we constructed a numerical scheme to solve the non-hydrostatic model. To investigate the accuracy of the models, benchmark tests comparing the computed results with experimental data were conducted in Section 4. Conclusions and remarks will be given in the last section.

2 Governing Equations

In this section, we consider the one-layer non-hydrostatic model, which is used to simulate the free surface waves generated by dam-break flow through various obstacles.

Suppose a fluid layer bounded below by a topography $d(x)$ and above by the free surface $\eta(x,t)$, flowing through an open channel with a rectangular cross-section as sketched in Figure 1. The motion of the free surface is governed by the one layer non-hydrostatic Saint Venant equations given by the followings

$$\frac{\partial A}{\partial t} + \frac{\partial Q}{\partial x} = 0, \tag{1}$$

$$\frac{\partial \hat{u}}{\partial t} + \hat{u}\frac{\partial \hat{u}}{\partial x} + g\frac{\partial(\hat{h}+\hat{d})}{\partial x} = -\frac{1}{2}\frac{\partial p}{\partial x}, \tag{2}$$

$$\frac{1}{2}\left(\frac{\partial v_{top}}{\partial t} + \frac{\partial v_{bot}}{\partial t}\right) = \frac{p}{h}, \tag{3}$$

$$\frac{v_{top} - v_{bot}}{h} + \frac{\partial u}{\partial x} = 0, \tag{4}$$

$$v_{bot} = -u\frac{\partial d}{\partial x}, \tag{5}$$

If we neglect the pressure term $p(x,z,t)$, the continuity equations (1) and the momentum balances in x-direction (2) are the well-known hydrostatic Saint Venant equations. The equation (3) is the momentum balances in z-direction while the equation (4) is the depth integrated continuity equation. The last equation (5) is a kinematic condition for fixed bottom $d(x)$, see [28] for time-varying bottom.

The notations $A(x,t)$ represents the wet cross-sectional area of the channel whereas the notation $Q(x,t)$ is flux or discharge. Note that $Q(x,t) = A(x,t)\hat{u}(x,t)$, with $\hat{u}(x,t)$ is the horizontal fluid velocity. Because we consider the case of rectangular channels, thus the cross-section area has the following relation $A(x,t) = \hat{h}\hat{b}$, with $\hat{h}(x,t)$ denotes the fluid height, and $\hat{b}(x)$ the channel width. Furthermore, the vertical fluid velocity on the free surface and the bottom are represented by v_{top} and v_{bot} respectively. On the free surface, the hydrodynamic pressure is zero $p(x,t) = 0$, whereas at the bottom is non-zero.

3 Numerical Method

In this section, we revisited a numerical scheme for the hydrodynamic model using the MCS.

Consider equations (1)-(5) on the spatial domain $\Omega = [x_{min}, x_{max}]$ and time interval $\tau = [0, T]$ with boundary prescribed in the downstream. The time interval τ is divided into N_t number of time interval partitions with time steps length of Δt and for all $n \in I_n$, $I_n = \{0, 1, 2, ..., N_t\}$, $t^n = n\Delta t$. The spatial domain Ω is divided into N_x number of cells with a spatial length of $\Delta x/2$ to obtain a staggered grid with partition points $P = \{x_{j+1/2}\}_{j\in I}$ and for all $j \in I = \{0, 1, 2, ..., N_x\}, x_{j+1/2} = (j + \frac{1}{2})\Delta x$. This
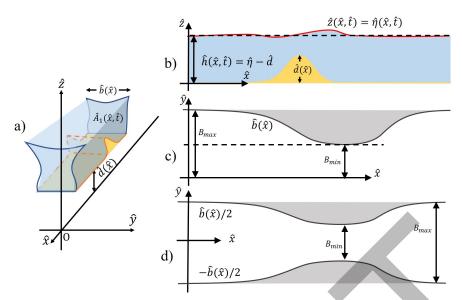
Figure 1: Sketch of domain and notation: (a) 3D view of open channel flow, (b) top view, (c) side view of channel width $b(x)$ and (d) side view of the channel walls visualize as $y = \pm b(x)/2$

staggered arrangement allows us to calculate the unknown on neighbouring grid points alternately, e.g. $u(x_{j+1/2}, t^n) = u_{j+1/2}^n$ is approximated on the half grid points, whereas $a(x_j, t^n) = a_j^n$, $p(x_j, t^n) = p_j^n$ and $v(x_j, t^n)|_{\text{top[bot]}} = v_{j,\text{top[bot]}}^n$ is approximated on the full grid points. Thus the fully discrete scheme is

$$A_j^{n+1} = A_j^n - \frac{\Delta t}{\Delta x}\left(Q_{j+1/2}^n - Q_{j-1/2}^n\right), \quad (6)$$

$$u_{j+1/2}^{n+1} = u_{j+1/2}^n - \Delta t (uu_x)_{j+1/2}^n \cdots$$
$$- g\frac{\Delta t}{\Delta x}\left(\eta_{j+1}^{n+1} - \eta_j^{n+1}\right)\cdots$$
$$- \frac{\Delta t}{2\Delta x}\left(p_{j+1}^{n+1} - p_j^{n+1}\right), \quad (7)$$

$$v_{j,\text{top}}^{n+1} = v_{j,\text{top}}^n - \left(v_{j,\text{bot}}^{n+1} - v_{j,\text{bot}}^n\right)\cdots$$
$$+ 2\Delta t \frac{p_j^{n+1}}{h_j^{n+1}}, \quad (8)$$

$$v_{j,\text{top}}^{n+1} + h_j^{n+1}\frac{u_{j+1/2}^{n+1} - u_{j-1/2}^{n+1}}{\Delta x} = v_{j,\text{bot}}^{n+1}, \quad (9)$$

$$v_{j,\text{bot}}^{n+1} = -\max\left(0, u_{j-1/2}^n\right)\frac{d_j - d_{j-1}}{\Delta x}\cdots$$
$$- \min\left(0, u_{j+1/2}^n\right)\frac{d_{j+1} - d_j}{\Delta x}. \quad (10)$$

In the following, the unknown variables are computed consistently

$$A|_j = h|_j b|_j, \quad Q|_{j+1/2} = {}^* A_{j+1/2} b_j, \quad (11)$$

where ${}^* A_{j+1/2}$ is calculated using the upwind approx-

imation,

$${}^* A_{j+1/2} = \begin{cases} h_j b_j, & \text{for} \quad u_{j+1/2} \geq 0, \\ h_{j+1} b_{j+1}, & \text{for} \quad u_{j+1/2} < 0. \end{cases} \quad (12)$$

The term advection is approximated by the momentum conservative principle as first proposed in [22], and then modified by several authors [26, 25] to consider the wet-cross sectional area as follows

$$uu_x = \frac{1}{A}(Qu)_x - \frac{1}{A}uQ_x. \quad (13)$$

Adopting the relation (13), the consistent approximation for the advection term reads as follows

$$uu_x|_{j+\frac{1}{2}} = \frac{1}{\bar{A}_{j+1/2}}\left(\frac{\bar{Q}_{j+1}{}^* u_{j+1} - \bar{Q}_j{}^* u_j}{\Delta x}\right)$$
$$- \frac{1}{\bar{A}_{j+1/2}}\left(u_{j+1/2}\frac{\bar{Q}_{j+1} - \bar{Q}_j}{\Delta x}\right), \quad (14)$$

whereas

$$\bar{A}_{j+1/2} = \frac{A_j + A_{j+1}}{2}, \quad \bar{Q}_j = \frac{Q_{j-1/2} + Q_{j+1/2}}{2}, \quad (15)$$

and the first-order upwind approximation for horizontal velocity,

$${}^* u_j = \begin{cases} u_{j-1/2}, & \text{for} \quad \bar{Q}_j \geq 0, \\ u_{j+1/2}, & \text{for} \quad \bar{Q}_j < 0. \end{cases} \quad (16)$$

There are five unknown in the non-linear system equations (6)-(10) such as $(A_j^{n+1}, u_{j+1/2}^{n+1}, v_{j,\text{top}}^{n+1}, v_{j,\text{bot}}^{n+1}, p_j^{n+1})$, that must be calculated. To obtain the solution, we substitute the equations (7)-(8) into equation (9) to yields the Poisson pressure equation

$$\mathbf{A}\vec{p}^{n+1} = \vec{f} \quad (17)$$

where

$$\mathbf{A} = \begin{bmatrix} a_1 & b_1 & & & & \\ c_2 & a_2 & b_2 & & & \mathbf{0} \\ & c_3 & a_3 & b_3 & & \\ & & \ddots & \ddots & \ddots & \\ \mathbf{0} & & & c_{Nx-1} & a_{Nx-1} & b_{Nx-1} \\ & & & & c_{Nx} & a_{Nx} \end{bmatrix},$$

$$p = \begin{bmatrix} p_1^{n+1} \\ p_2^{n+1} \\ p_3^{n+1} \\ \vdots \\ p_{Nx-1}^{n+1} \\ p_{Nx}^{n+1} \end{bmatrix}, \quad f = \begin{bmatrix} f_1 \\ f_2 \\ f_3 \\ \vdots \\ f_{Nx-1} \\ f_{Nx} \end{bmatrix},$$

$$a_i = \frac{\Delta t}{\Delta x} h_j^{n+1} + \frac{2\Delta x \Delta t}{h_j^{n+1}}, \quad b_i = -\frac{\Delta t}{2\Delta x} h_j^{n+1},$$

$$c_i = b_i,$$

$$f_i = -h_j^{n+1}\left(\hat{u}_{j+1/2} - \hat{u}_{j-1/2} \right) \cdots$$

$$- \Delta x \left(v_{j,\text{top}}^n + v_{j,\text{bot}}^n \right) + 2\Delta x v_{j,\text{bot}}^{n+1}$$

The tridiagonal matrix A is $N_x \times N_x$ in the system of linear equations (17) for which can be solved by any tridiagonal matrix solver, for example Thomas Algoritm, hence it is very efficient.

Next, we use predictor-corrector procedure to obtain the values of $u_{j+1/2}$ at each time step. First we solve equation (7) without hydrodynamic pressure term as predictor procedure and the solution is denoted by $\hat{u}_{j+1/2}$. In correction procedure, we update the value using the following formula

$$u_{j+1/2}^{n+1} = \hat{u}_{j+1/2}^{n+1} - \frac{\Delta t}{2\Delta x}\left(p_{j+1}^{n+1} - p_j^{n+1} \right). \quad (18)$$

We summarize the procedure to solve the one layer non-hydrostatic Saint Venat model given as follows

---
Algorithm 1 NH-1L Saint Venant

Input: initial condition, specific topography $d(x)$ or channel width $b(x)$
Output: water level h_j^n
Proccedure:
1: Solve the hydrostatic Saint Venant model using the MCS scheme. From the equation (6) we get A_j^{n+1} then using relation (11) we get h_j^{n+1}. Meanwhile, from the equation (7) we get the predicted value $\hat{u}_{j+1/2}^{n+1}$,
2: Solve the Poisson pressure equation (17) using Thomas Algoritm to get p_j^{n+1},
3: Calculate $v_{j,\text{bot}}^{n+1}$ using equation (10),
4: Calculate $u_{j+1/2}^{n+1}$ using corrector procedure (18),
5: Calculate $v_{j,\text{top}}^{n+1}$ using equation (8)

Another version of this one-layer non-hydrostatic model can be found in [18] and [28].

Dam-break simulations often encounter problems in the wet-dry transition area. Thus, a simple wet-dry procedure combined with a thin-layer technique should be employed. If the entire water depth in the dry region is less than the provided threshold value h_{thin}, the initial water depth is replaced by a thin layer of water with depth h_{thin}, specifically.

$$h = \begin{cases} h_j^n, & \text{for } h_j^n \geq h_{thin}, \\ h_{thin}, & \text{for } h_j^n < h_{thin}. \end{cases} \quad (19)$$

Moreover, in the dry area, the momentum balance equation (7) is turned off to avoid numerical instability. In this case, a cell is deemed dry if the water level is less than the threshold value or if the area A_j in (15) is less than the threshold value A_{thres} given beforehand.

4 Results and Discussion

In this section, we will investigate the capability of our proposed scheme to study the dam-break flow through different obstacles; bottom obstacles and channel wall contractions obstacles. In this simulation, the friction term are considered by adding the friction term $-C_f|u|u$ in the R.H.S of momentum balance in x-direction (2), as follows

$$C_f = \frac{gN^2}{h^{1/3}} \quad (20)$$

where, C_f is the drag coefficient parameter, expressed in terms of the Manning coefficient N.

4.1 Channel Wall Contraction Obstacles

The dam-break flow laboratory experiment through a channel with various contraction geometries was conducted by [10]. The experiment was conducted in a rectangular horizontal channel 8.90 m long, 0.30 m broad, and 0.34 m high as sketched in Figure 2a. The fluid reservoir in the upstream part was constructed and initially filled with water to a depth of $h_0 = 0.25$ m. The vertical gate (red) symbolizing the dam, situated 4.65 m from the left boundary. The 4.25 m long downstream part of the channel was initially dry, and the right boundary is open boundary so that the flow can descend freely without reflection, as shown in Figure 2b. Here, three types of contractions were build in the form of trapezoid and triangular contractions. There are two types of trapezoidal contraction with different dimension, referred as trapezoidal A and B, and one triangular contraction. Three type of contractions which located at the contraction zone indicate a transition from smooth (represented by trapezoidal A and B contractions) to abrupt contraction (represented by triangle contractions), as shown in Figure 2c. To investigate the contraction effect, in each experiment, the lengths of the contraction zone were 0.95 m, the maximum contraction width was 0.10 m, and the distance from the gate was 1.52 m.
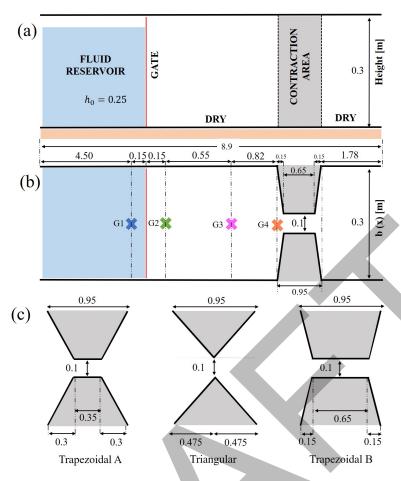
Figure 2: Experiment configuration; (a) side view, (b) top view of the channel along with locations of the four gauges are indicated by crosses: G1 (blue), G2 (green), G3 (magenta), and G4 (brown). (c) Top view of the three contraction models and their dimensions (in meters), redrawn from [26, 10].
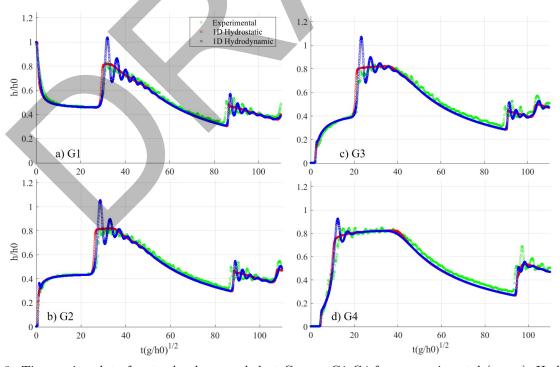

Figure 3: Time series plot of water levels, recorded at Gauges G1-G4 from experimental (green), Hydrostatic (red) and Hydrodynamic (blue), for channel with Trapezoidal B contraction.
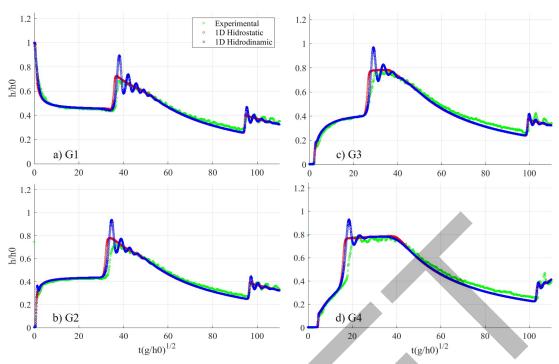
Figure 4: Time series plot of water levels, recorded at Gauges G1-G4 from experimental (green), Hydrostatic (red) and Hydrodynamic (blue), for channel with triangular contraction.
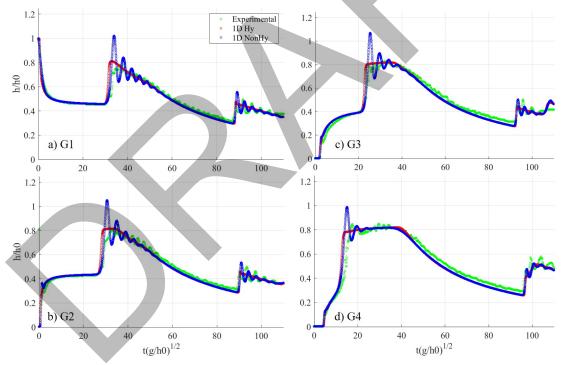

Figure 5: Time series plot of water levels, recorded at Gauges G1-G4 from experimental (green), Hydrostatic (red) and Hydrodynamic (blue), for channel with trapezoidal A contraction.

Numerical simulations are performed with the following set-up; wet-dry threshold $A_{thres} = 0.001$, thin film technique $h_{thin} = 0.0001$, drag coefficient $C_f = 0.0026$, spatial step $\Delta x = 0.05$ and CFL-like condition $C = 0.2$. Simulations are conducted by using initial conditions as follows; initial horizontal velocity $u(x, 0) = 0$, initial flux $Q(x, 0) = 0$, initial vertical velocity $w(x, 0) = 0$, initial water level $h_0 = 0.25$ m on

the upstream part of the reservoir, and h_{thin} on the downstream part of the channel to accommodate the dry situation. The bottom topography $\hat{d}(\hat{x})$ is flat bottom, see Figure 2a. Moreover, the channel width $\hat{b}(\hat{x})$ is varying where the profile is visualize as $y = \pm \hat{b}(\hat{x})/2$ sketched in Figure 2b.

The simulation results (red) from our previous contribution [25] were compared to experimental data
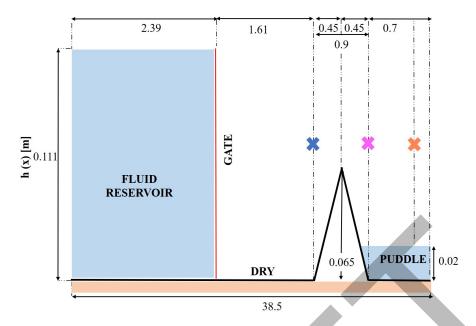
Figure 6: Experiment configuration of Dam-break through the triangular bottom obstacle. The top view of the channel along with the locations of the three gauges are indicated by crosses: G1 (blue), G2 (magenta), and G3 (brown), redrawn from [20].

(green) at four gauge locations for trapezoidal type A contraction (Figure 5), trapezoidal type B contraction (Figure 3), and triangular contraction (Figure 4). The simulation results are presented in the form of normalized water level h/h_0 on the vertical axis y versus normalized time $t(gh_0)^{1/2}$ on the horizontal axis x. It is shown that the hydrostatic model successfully predicts hydraulic jumps in the three types of channels which is in line with [14] results, but unable to capture the oscillating dispersive wave train at the locations where hydraulic jumps occur. This indicates that dispersive effects cannot be captured using hydrostatic models. The results from our hydrodynamics model (blue), on the other hand demonstrates the evolution of a negative wave displacement followed by a dispersive wave train with oscillation appearing in the location where the hydraulic jump occurs. Even though the oscillations are slightly over fitting, probably due to the absence of turbulence nor use any viscosity term [10], they are still acceptable with the RMSE error less than 4.458%.

4.2 Bottom Obstacle

The laboratory experiment through a rectangular horizontal channel with bottom triangular obstacle was conducted by [20]. It is a 5.60 m long, 0.5 m broad, and 0.11 m high as sketched in Figure 6. The water barrier (gate) is located 2.39 m from the upstream to form a fluid reservoir, initially filled with water with $h_0 = 0.111$m height. The triangular bottom obstacle with 0.065 m height, 0.9 m long and and has bed slopes of ± 0.14 is located 1.61m from the gate, to form a still water puddle downstream of the channel. The puddle downstream is 0.02m in height where the right boundary is hard-wall glass.

Numerical simulations are performed with the following set-up; wet-dry threshold $A_{thres} = 0.0001$, thin film technique $h_{thin} = 0.0001$, Manning coefficient $N = 0.011$, spatial step $\Delta x = 0.025$ and CFL-like condition $C = 0.1$. Simulations are conducted by using initial conditions as follows; initial horizontal velocity $u(x,0) = 0$, initial flux $Q(x,0) = 0$, initial vertical velocity $w(x,0) = 0$ and h_{thin} on the part of the channel to accommodate the dry situation. The bottom topography $\hat{d}(\hat{x})$ is triangular bottom, see Figure 6. Moreover, the channel width is straight wall which is $\hat{b}(\hat{x}) = 1$.

As before, for the three gauge sites depicted in Figure 7, the results using the hydrostatic (red) were presented alongside the hydrodynamic (blue) and compared with the experimental data (green). The hydrostatic model is able to accurately forecast hydraulic jumps, which is consistent with the findings of [14], but it is unable to account for dispersive phenomena at the places where hydraulic jumps occur, as seen in Figure 7. For example in G1, the dispersive wave train located at the hydraulics jump at normalized time $0 < t(gh_0)^{1/2} < 5$ is unable to be simulated by our hydrostatic model as well as the result on [14], but it can be captured very well by non-hydrostatic model. In contrast to the previous contraction case, the over fitting problem in wave train oscillations is not visible in the simulation results with the triangular botom obstacle. Further, the numerical result are compared with the experimental and accurate enough with the acceptable RMSE error less than 3.3756%. This demonstrates both the appropriate of the numerical treatment of dispersive terms in our model and the ability of our non-hydrostatic (hydrodynamic) model to describe dispersive phenomena.
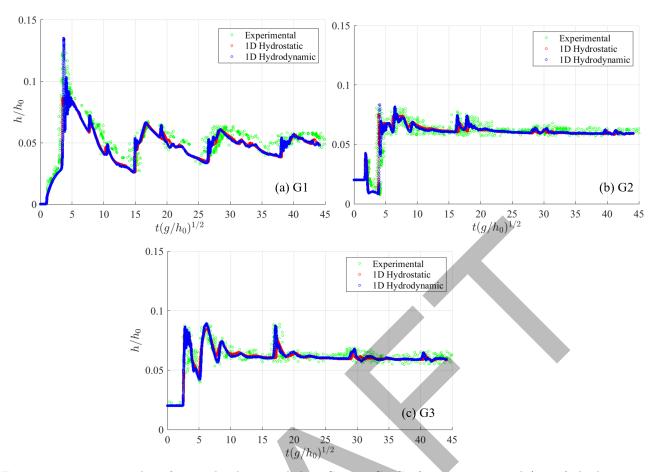
Figure 7: Time series plot of water levels, recorded at Gauges G1-G3 from experimental (green), hydrostatic (red) and hydrodynamic (blue) for simulation with bottom triangular obstacles.

5   Conclusion

We have successfully extended a one-layer non-hydrostatic numerical scheme for study dam-break flow in an open channel by solving one layer non-hydrostatic Saint Venant equation. Our scheme is capable to simulate surface waves due to dam-break flow through various obstacles including triangular bottom and channel wall obstacle. It is able to predict the negative wave displacement followed by an oscillating dispersive wave train, indicating that dispersive phenomena are well captured. For simulations with triangular bottom obstacle, the simulation results reveal that our scheme can handle dispersive wave trains and hydraulic jumps simultaneously, where this feature is not available in the previous hydrostatic model. We conclude that the hydrodynamic pressure term should be considered in the model and the appropriate of the numerical treatment must be carefully implemented. Our numerical finding is consistent with experimental data with the acceptable RMSE error. Furthermore, our scheme is efficient because it only solves one vertical layer and, in terms of computation we only need to calculate the Poisson pressure component with a tridiagonal matrix coefficient for each time step. Moreover we expect that our alternative models will be computationally competitive with dispersive models such as KdV or Boussinesq, and

will be adequate for usage by civil engineers working on dam designs, river normalization, and risk disaster management.

References

[1] AL-GHOSOUN, A., EL MOÇAYD, N., AND SEAID, M. A surrogate model for efficient quantification of uncertainties in multilayer shallow water flows. *Environmental Modelling & Software 144* (Oct. 2021), 105176.

[2] CAI, S., MAO, Z., WANG, Z., YIN, M., AND KARNIADAKIS, G. E. Physics-informed neural networks (PINNs) for fluid mechanics: a review. *Acta Mech. Sin. 37*, 12 (Dec. 2021), 1727–1738.

[3] CANTERO-CHINCHILLA, F. N., CASTRO-ORGAZ, O., DEY, S., AND AYUSO, J. L. Nonhydrostatic Dam Break Flows. I: Physical Equations and Nu-

merical Schemes. *J. Hydraul. Eng. 142*, 12 (Dec. 2016), 04016068.

[4] CAO, Z., HUANG, W., PENDER, G., AND LIU, X. Even more destructive: cascade dam break floods: Cascade dam break floods. *Journal of Flood Risk Management 7*, 4, 357–373.

[5] DAI, S., HE, Y., YANG, J., MA, Y., JIN, S., AND LIANG, C. Numerical study of cascading dam-break characteristics using SWEs and RANS. *Water Supply 20*, 1, 348–360.

[6] DARIPA, P. Higher-order boussinesq equations for two-way propagation of shallow water waves. *European Journal of Mechanics - B/Fluids 25*, 6, 1008–1021.

[7] HU, H., ZHANG, J., AND LI, T. Dam-break flows: Comparison between flow-3d, MIKE 3 FM, and analytical solutions with experimental data. *Applied Sciences 8*, 12, 2456.

[8] HU, H., ZHANG, J., LI, T., AND YANG, J. A simplified mathematical model for the dam-breach hydrograph for three reservoir geometries following a sudden full dam break. *Natural Hazards 102*, 3, 1515–1540.

[9] KIM, D.-H., AND LYNETT, P. J. Dispersive and Nonhydrostatic Pressure Effects at the Front of Surge. *J. Hydraul. Eng. 137*, 7 (July 2011), 754–765.

[10] KOCAMAN, S., GÜZEL, H., EVANGELISTA, S., OZMEN-CAGATAY, H., AND VICCIONE, G. Experimental and numerical analysis of a dam-break flow through different contraction geometries of the channel. *Water (Switzerland) 12*, 4 (2020).

[11] KUDELA, J., AND MATOUSEK, R. Recent advances and applications of surrogate models for finite element method computations: a review. *Soft Comput 26*, 24 (Dec. 2022), 13709–13733.

[12] KUDELA, J., AND MATOUSEK, R. Combining Lipschitz and RBF Surrogate Models for High-dimensional Computationally Expensive Problems. *Information Sciences 619* (Jan. 2023), 457–477. arXiv:2204.14236 [cs, math].

[13] LI, J., CAO, Z., PENDER, G., AND LIU, Q. A double layer-averaged model for dam-break flows over mobile bed. *Journal of Hydraulic Research 51*, 5, 518–534.

[14] MAGDALENA, I., HARIZ, A., FARID, M., AND KUSUMA, M. S. B. Numerical studies using staggered finite volume for dam break flow with an obstacle through different geometries. *Results in Applied Mathematics 12* (2021), 100193.

[15] MOHAPATRA, P. K., AND CHAUDHRY, M. H. Numerical solution of boussinesq equations to simulate dam-break flows. *J. Hydraul. Eng. 130*, 2, 156–159.

[16] NGUYEN, V. M., PHAN, H. N., AND PHAN, T. H. Prediction of Unstable Hydrodynamic Forces on Submerged Structures under the Water Surface Using a Data-Driven Modeling Approach. *Buildings 12*, 10 (Oct. 2022), 1683.

[17] OZMEN-CAGATAY, H., AND KOCAMAN, S. Dam-break flows during initial stage using SWE and RANS approaches. *Journal of Hydraulic Research 48*, 5, 603–611.

[18] PUDJAPRASETYA, S. R., AND TJANDRA, S. A Hydrodynamic Model for Dispersive Waves Generated by Bottom Motion. *Springer Proceedings in Mathematics and Statistics 77* (2014).

[19] QIAN, H., CAO, Z., LIU, H., AND PENDER, G. New experimental dataset for partial dam-break floods over mobile beds. *Journal of Hydraulic Research 56*, 1, 124–135.

[20] SOARES-FRAZÃO, S. Experiments of dam-break wave over a triangular bottom sill. *Journal of Hydraulic Research 45*, 19–26.

[21] SOARES-FRAZÃO, S., AND GUINOT, V. A second-order semi-implicit hybrid scheme for one-dimensional Boussinesq-type waves in rectangular channels. *Int. J. Numer. Meth. Fluids 58*, 3 (Sept. 2008), 237–261.

[22] STELLING, G., AND ZIJLEMA, M. An accurate and effcient finite-difference algorithm for non-hydrostatic free-surface flow with application to wave propagation. *International Journal for Numerical Methods in Fluids 23*, May 2002 (2003), 1–23.

[23] SUN, J., LI, X., YANG, Q., TIAN, Y., WANG, S., AND YANG, M. Hydrodynamic numerical simulations based on residual cooperative neural network. *Advances in Water Resources 180* (2023), 104523.

[24] S.V. LUND, N., MADSEN, H., MAZZOLENI, M., SOLOMATINE, D., AND BORUP, M. Assimilating flow and level data into an urban drainage surrogate model for forecasting flows and overflows. *Journal of Environmental Management 248* (Oct. 2019), 109052.

[25] SWASTIKA, P. V., AND PUDJAPRASETYA, S. R. The Momentum Conserving Scheme Implementation for Simulating Dambreak Flow in a Channel with Various Contractions. In *IOP Conference Series: Earth and Environmental Science* (2021), vol. 925, p. 012012.

[26] Swastika, P. V., Pudjaprasetya, S. R., Wiryanto, L. H., and Hadiarti, R. N. A momentum-conserving scheme for flow simulation in 1D channel with obstacle and contraction. *Fluids 6*, 1 (2021), 26.

[27] Tang, S., Feng, X., Wu, W., and Xu, H. Physics-informed neural networks combined with polynomial interpolation to solve nonlinear partial differential equations. *Computers & Mathematics with Applications 132* (2023), 48–62.

[28] Tarwidi, D., Pudjaprasetya, S. R., and Tjandra, S. S. A Non-Hydrostatic Model for Simulating Weakly Dispersive Landslide-Generated Waves. *Water 15*, 4 (Feb. 2023), 652.

[29] Wang, J., Liang, D., Zhang, J., and Xiao, Y. Comparison between shallow water and boussinesq models for predicting cascading dam-break flows. *Natural Hazards 83*, 1, 327–343.

[30] Zhang, Y., and Lin, P. An improved SWE model for simulation of dam-break flows. *Proceedings of the Institution of Civil Engineers - Water Management 169*, 6, 260–274.